Proceedings of IMECE'00
2000 International Mechanical Engineering Congress and Exhibition
November 5-10, 2000, Orlando, Florida, USA

2000 IMECE 2-13-2-7

NUMERICAL SIMULATION OF CONDENSATION ON A CAPILLARY GROOVED STRUCTURE

Yuwen Zhang[1] and Amir Faghri
Department of Mechanical Engineering
University of Connecticut
Storrs, Connecticut 06269
Email: zhangy12@asme.org

ABSTRACT

Condensation in a capillary grooved structure is investigated using the Volume of Fluid (VOF) model. The governing equations are written in a generalized form and are applicable to both liquid and vapor phases. Condensation on the fin top and at the meniscus is modeled by introducing additional source terms in the continuity, VOF, and energy equations. The effects of temperature drop, contact angle, surface tension, and fin thickness on the condensation heat transfer are investigated.

NOMENCLATURE

c_p	specific heat, $J/(kgK)$
F	body force, N
h	enthalpy, J/kg
h_c	heat transfer coefficient, $W/(m^2K)$
h_{fg}	latent heat of condensation, J/kg
k	thermal conductivity, $W/(mK)$
L_1	one half of the fin thickness, m
$\dot{m}$	mass flow rate (kg/s)
$\dot{m}'''$	condensation rate at the meniscus, $kg/(m^3s)$
p	pressure, Pa
q	local heat flux, W/m^2
$S_{\Delta H}$	source term, W/m^3
T	temperature, K
t_g	height of the fin, m
t_v	height of the vapor space, m
u, v	velocity components in the x, y direction, m/s
W	one half of the the groove width, m
x, y	coordinate, m

Greek symbols

δ	film thickness on the fin top, m
ΔT	temperature difference, $T_{sat} - T_0$, K
ε	volume fraction of liquid
θ_{men}	menisicus contact angle
μ	dynamic viscosity, Pa·s
ρ	density, kg/m^3
σ	surface tension, N/m

Subscripts

0	bottom of the fin
f	fin
ℓ	liquid
men	meniscus
sat	saturation
v	vapor

INTRODUCTION

Vapor condensation in capillary grooves, pores and slots is very important for many two-phase devices such as heat pipes, condensers, etc. The vapor condenses because the solid wall temperature is below the vapor saturation temperature. Heat transfer during condensation from the liquid-vapor meniscus in these structures is very important for predicting performance of two-phase devices. Khrustalev and Faghri (1994a) analyzed heat transfer of a micro heat pipe with triangular cross section. At the condenser section of the heat pipe, liquid resides in the corner of the triangular cross section due to capillary pressure. The vapor condenses at these inner surfaces of the triangle, and the condensate is sucked into the corner of the triangle. The

[1]Presently at Thermoflow, Inc., 29 Hudson Rd., Sudbury, MA 01776

thickness of the film was described using an ordinary differential equation proposed by Kamotani (1976) together with an assumption of polynomial film thickness variation. Khrustalev and Faghri (1994b) investigated heat transfer during evaporation and condensation on capillary grooved structures of heat pipes. Effects of disjoining pressure and interfacial thermal resistance on the film condensation on the fin top surface were taken into account in their model. Their numerical results indicated that the effect of interfacial thermal resistance is negligible because the film thickness is comparatively large. The vapor was assumed to be saturated and the effect of vapor superheat on condensation was not taken into account. In addition, heat transfer in the liquid residing in the grooves was modeled as purely a conduction problem by Khrustalev and Faghri (1994a,b). Khrustalev and Faghri (1996) investigated fluid flow effects on evaporation from the liquid vapor meniscus. Heat conduction in the solid wall was neglected based on the argument that the thermal conductivity of the solid wall is much higher than that of working fluid. They concluded that fluid flow can be very important when the temperature difference is large.

The objective of the present study is to investigate condensation at the liquid vapor meniscus in a capillary groove. The successful solutiou of the problem requires the numerical solutions of: (1) film condensation on the fin top; (2) condensation at the liquid vapor meniscus; and (3) fluid flow in the capillary groove. The effects of cooling temperature, contact angle, surface tension, and fin geometry on the condensation will also be investigated.

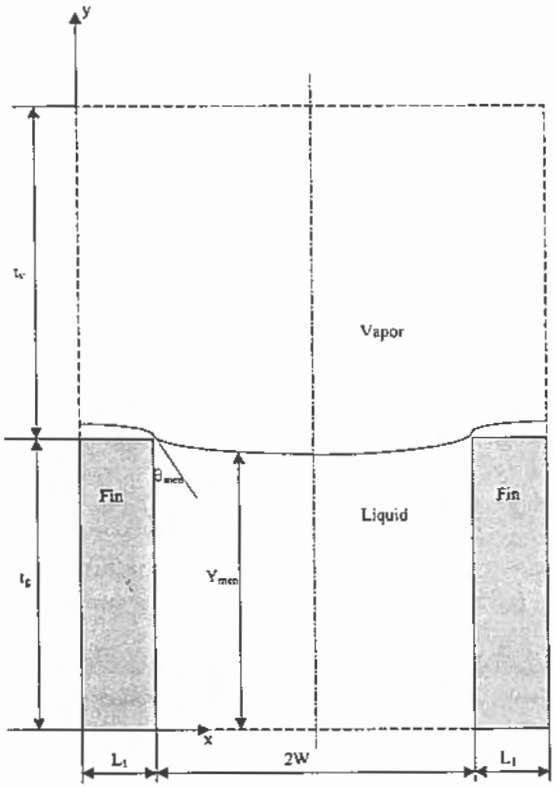

Figure 1. Geometric configuration of the capillary groove

PHYSICAL MODEL

The condensation of the vapor at the liquid-vapor meniscus interface is shown in Fig. 1. It can be considered as a capillary groove or pore structure in the condenser. In order to solve the problem, the following assumptions are made:

1. Since the width of the groove is very small, the effect of gravity can be neglected due to surface tension dominance.
2. The number of the grooves is large enough so that symmetry conditions are applicable at the left and right side of the domain (Khrustalev and Faghri, 1999).
3. The temperature in the fin is uniformly equal to the cooling temperature, T_w. This assumption is justified because the thermal conductivity of the fin is several hundred times higher than that of the liquid working fluid (Khrustalev and Faghri, 1994b; 1996).
4. The liquid and vapor flow are laminar and incompressible.
5. The thermal properties of liquid and vapor are not dependents of temperature..

Governing equations

Since heat transfer and fluid flow is a symmetric problem, only half of the groove needs to he investigated. In order to simplify the solving procedure, one set of the governing equations is written for hoth the liquid and vapor regions. The continuity and momentum equations are

$$\frac{D\rho}{Dt} + \rho\left(\frac{\partial u}{\partial x} + \frac{\partial v}{\partial y}\right) = 0 \qquad (1)$$

$$\rho\left(\frac{\partial u}{\partial t} + u\frac{\partial u}{\partial x} + v\frac{\partial u}{\partial y}\right) = -\frac{\partial p}{\partial x} + \mu\left(\frac{\partial^2 u}{\partial x^2} + \frac{\partial^2 u}{\partial y^2}\right) + F_x \qquad (2)$$

$$\rho\left(\frac{\partial v}{\partial t}+u\frac{\partial v}{\partial x}+v\frac{\partial v}{\partial y}\right)=-\frac{\partial p}{\partial y}+\mu\left(\frac{\partial^2 v}{\partial x^2}+\frac{\partial^2 v}{\partial y^2}\right)+F_y \quad (3)$$

where F_x and F_y are the components of the body force resulting from surface tension at the interface and will be described later. The fluid properties are defined as

$$\rho=(1-\epsilon_\ell)\rho_v+\epsilon_\ell\rho_\ell \quad (4)$$

$$\mu=(1-\epsilon_\ell)\mu_v+\epsilon_\ell\mu_\ell \quad (5)$$

and ϵ_ℓ is volume fraction of liquid. The value of ϵ_ℓ is zero in the vapor phase and unity in the liquid phase. The volume fraction of water, ϵ_ℓ, satisfies the continuity equation for the liquid phase

$$\frac{D\epsilon_\ell}{Dt}+\epsilon_\ell\left(\frac{\partial u}{\partial x}+\frac{\partial v}{\partial y}\right)=\frac{\dot{m}'''}{\rho_\ell} \quad (6)$$

where $\dot{m}'''$ represents the mass production rate of condensation.

Equation (6) can be rewritten as

$$\frac{D\epsilon_\ell}{Dt}=\frac{\dot{m}'''}{\rho_\ell}-\epsilon_\ell\left(\frac{\partial u}{\partial x}+\frac{\partial v}{\partial y}\right)=S_{\epsilon_\ell} \quad (7)$$

Similarly, the volume fraction of vapor, ϵ_v, satisfies the following equation

$$\frac{D\epsilon_v}{Dt}+\epsilon_v\nabla\cdot\mathbf{V}=-\frac{\dot{m}'''}{\rho_v} \quad (8)$$

Substituting eq. (4) into eq. (1) and considering eq. (6), the continuity equation is simplified

$$\frac{\partial u}{\partial x}+\frac{\partial v}{\partial y}=-\left(\frac{1}{\rho_v}-\frac{1}{\rho_\ell}\right)\dot{m}''' \quad (9)$$

Substituting eq. (9) into eq. (7), and obtaining the VOF equation

$$\frac{D\epsilon_\ell}{Dt}=\frac{\dot{m}'''}{\rho_\ell}-\epsilon_\ell\,\dot{m}'''\left(\frac{1}{\rho_v}-\frac{1}{\rho_\ell}\right)=S_{\epsilon\ell} \quad (10)$$

The thermal conductivity and specific heat can be defined using a similar method by which density is defined

$$k=(1-\epsilon_\ell)k_v+\epsilon_\ell k_\ell \quad (11)$$

The specific heat is defined using the weight fraction of liquid and vapor:

$$c_p=\frac{1}{\rho}\left[(1-\epsilon)\rho_v c_{pv}+\epsilon\rho_\ell c_{p\ell}\right] \quad (12)$$

The total enthalpy is defined as

$$\begin{aligned}H&=\frac{1}{\rho}\left[(1-\epsilon)\rho_v(h_v+h_{fg})+\epsilon\rho_\ell h_\ell\right]\\&=\frac{1}{\rho}\left[(1-\epsilon)\rho_v h_v+\epsilon\rho_\ell h_\ell\right]+\frac{1}{\rho}(1-\epsilon)\rho_v h_{fg}\end{aligned} \quad (13)$$

The two terms in the right hand side of eq. (13) represent contributions of sensible enthalpy, h, and latent heat, ΔH, to the total enthalpy

$$h=\frac{1}{\rho}\left[(1-\epsilon)\rho_v h_v+\epsilon\rho_\ell h_\ell\right] \quad (13a)$$

$$\Delta H=\frac{1}{\rho}\left[(1-\epsilon)\rho_v h_v+\epsilon\rho_\ell h_\ell\right] \quad (13b)$$

the total enthalpy defined in eq. (13) can be rewritten in terms of sensible enthalpy and latent heat

$$H=h+\Delta H \quad (14)$$

The energy equation written in terms of enthalpy and temperature is:

$$\frac{\partial}{\partial x}(\rho u H) + \frac{\partial}{\partial y}(\rho v H) = \frac{\partial}{\partial x}\left(k\frac{\partial T}{\partial x}\right) + \frac{\partial}{\partial y}\left(k\frac{\partial T}{\partial y}\right) \quad (15)$$

Substituting eq. (14) into eq. (15), one can obtain

$$\frac{\partial}{\partial x}(\rho u h) + \frac{\partial}{\partial y}(\rho v h) = \frac{\partial}{\partial x}\left(k\frac{\partial T}{\partial x}\right) + \frac{\partial}{\partial y}\left(k\frac{\partial T}{\partial y}\right) + S_{\Delta H} \quad (16)$$

where

$$S_{\Delta H} = -\left[\frac{\partial}{\partial x}(\rho u \Delta H) + \frac{\partial}{\partial y}(\rho v \Delta H)\right] \quad (17)$$

It can be seen that an additional term appears in the right hand side of eq. (16). This term is to account for the effect of condensation in the energy equation. The term is zero everywhere except at the liquid vapor interface. The rate of condensation at the control volume cells that encloses the liquid-vapor interface can be expressed as

$$\dot{m}''' = \frac{S_{\Delta H}}{h_{fg}} \quad (18)$$

Boundary conditions

The temperature at the hottom of the groove is constant

$$T = T_0, \quad y = 0 \quad (19)$$

The temperature in the fin is uniformly equal to the temperature at the bottom of the groove

$$T = T_0, \quad 0 < y < t_g, \quad 0 < x < L_1 \quad (20)$$

The velocity at the bottom of the groove satisfies

$$u = 0, \quad y = 0 \quad (21)$$

$$\frac{\partial v}{\partial y} = 0, \quad y = 0 \quad (22)$$

The boundary conditions at the top of the computational domain are

$$T = T_{sat}, \quad y = t_g + t_v \quad (23)$$

$$u = 0, \quad y = t_g + t_v \quad (24)$$

$$v = v_{in}, \quad y = t_g + t_v \quad (25)$$

where v_{in} is vapor inlet velocity and its value depends on the amount of vapor condensed at the fin top and the meniscus.

The left and right boundaries of the domain ($x = 0, L_1+W$) satisfy the symmetric boundary condition, $u = 0$, $\partial v/\partial x = 0$, and $\partial T/\partial x = 0$.

Consideration of liquid-vapor interface

The conservation of normal and tangential momentum for the control volumes at the solid-liquid interface is automatically satisfied because the governing equations were

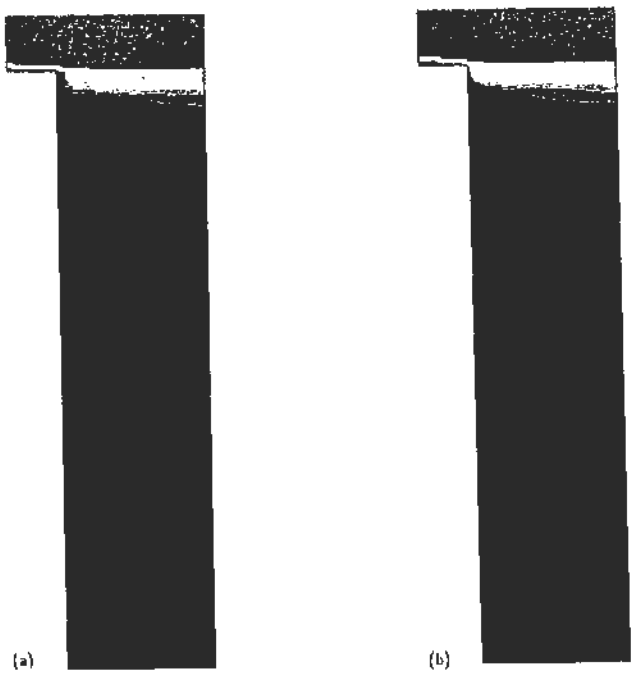

Figure 2. Water volume fraction: (a) $\Delta T = 5K$; (b) $\Delta T = 10K$

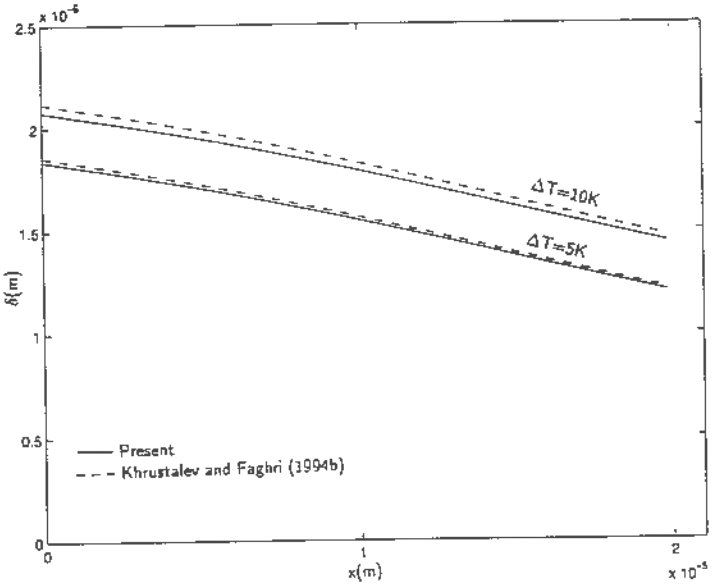

Figure 3. Comparison of liquid film thickness on the fin top

written for the entire computational domain, including liquid and vapor. The effect of surface tension on pressure is modeled using the continuous surface model. The model interprets surface tension as a continuous 3-D effect across the interface, rather than a boundary condition on the interface (Brackbill *et al.*, 1992). Forces due to the pressure jump at the interface can be expressed as volume force using the divergence theorem

$$\mathbf{F} = 2\sigma K \varepsilon_l \nabla \varepsilon_l \tag{26}$$

where curvature of the interface, K, is given by (Brackbill *et al.*, 1992)

$$K = \frac{1}{|\mathbf{n}|}\left[\left(\frac{\mathbf{n}}{|\mathbf{n}|}\cdot\nabla\right)|\mathbf{n}| - (\nabla\cdot\mathbf{n})\right] \tag{27}$$

The normal direction of the liquid vapor interface toward the vapor phase is n. The body force, F, obtained by eq. (26) is substituted into the momentum equations (2-3) to solve for the velocities in the liquid and vapor phases.

Liquid and vapor temperature are continuous at the interface. At the liquid vapor interface, the temperature should be equal to the saturation temperature.

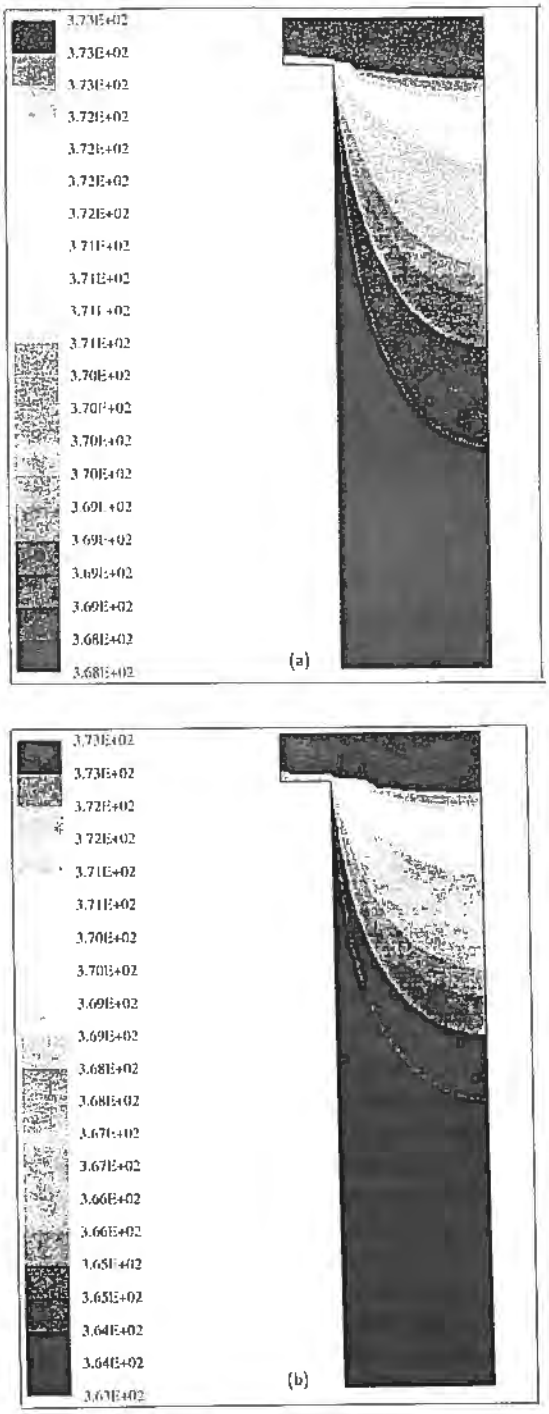

Figure 4. Temperature Contour: (a) $\Delta T = 5K$; (b) $\Delta T = 10K$

$$T = T_{sat}, \quad \begin{cases} y = t_g + \delta, & 0 < x < L_1 \\ y = Y_{men}, & L_1 < x < L_1 + W \end{cases} \tag{28}$$

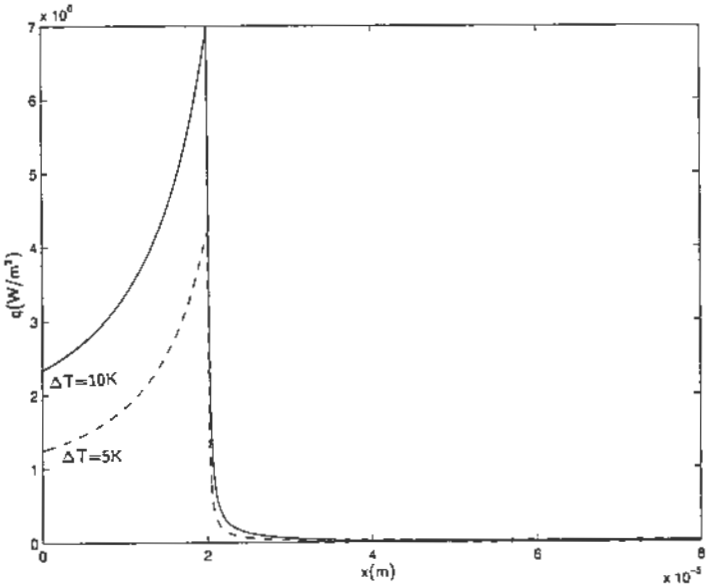

Figure 5. Local heat fluxes at different temperature

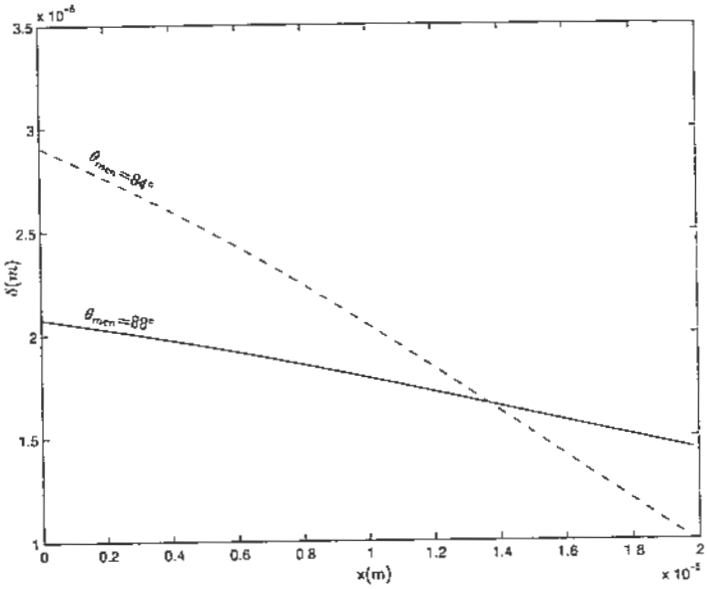

Figure 6. Effect of contact angle on the liquid film thickness

The sensible enthalpy corresponding to the above interface temperature is

$$h = c_p(T_{sat} - T_{ref}) \tag{29}$$

where T_{ref} is reference temperature of enthalpy.

The energy balance at the liquid vapor interface also needs to be satisfied. Since liquid and vapor regions are treated as one domain, the energy balance at the liquid vapor interface is satisfied when the converged solution for the entire domain is obtained.

NUMERICAL SOLUTION

In the numerical simulation, the interfacial temperature and enthalpy are set to the values specified in eqs. (28-29). The source term, $S_{\Delta H}$, that satisfies eqs. (28-29) is determined using eq. (16). Once the source term in the energy equation is determined, the condensation rate at the liquid-vapor interface can be determined using eq. (18).

The total condensation rate, which includes cnndensation at fin top and meniscus, is then expressed as

$$\dot{m} = \sum_{0<e<1} \dot{m}''' \, \Delta V \tag{30}$$

At steady state, this condensation rate can be used to determine vapor inlet velocity

$$v_{in} = \frac{\dot{m}}{\rho_v(L_1 + W)} \tag{31}$$

The effective condensation heat transfer coefficient is defined as follows

$$h_c = \frac{\dot{m}\, h_{fg}}{(L_1 + W)(T_{sat} - T_0)} \tag{32}$$

Here, only the steady-state solution of the condensation problem is investigated. It is impossible to solve the steady state problem directly, because the donor-acceptor model used in the VOF method works only for unsteady state problems. A false transient method (Basu and Srinivasan, 1988) is employed. With this methodology, the false transient terms are included in the governing equations and steady state is obtained when the condensation length does not vary with the false time. The overall numerical solution procedure for a particular time step is outlined below:

1. Assume a value for the mass production rate, $\dot{m}'''$ and

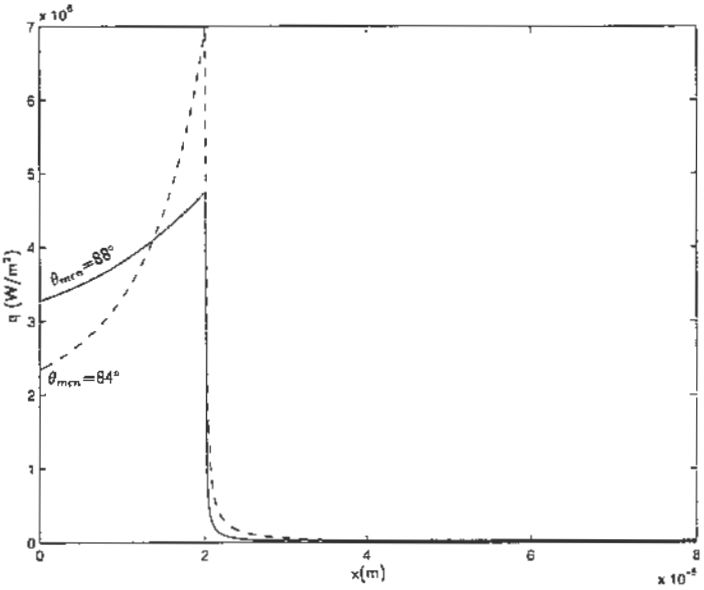

Figure 7. Effect of contact angle on the local heat fluxes

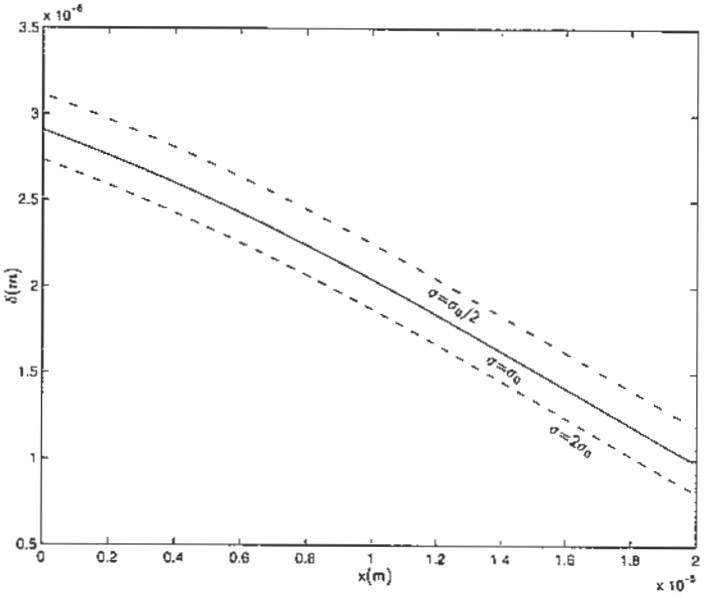

Figure 8. Effect of surface tension on the liquid film thickness

compute the source term for the VOF eq. (10) and the continuity eq. (9).

2. Calculate vapor inlet velocity, v_{in}, based on eqs. (30-31).
3. Solve the VOF eq. (10).
4. Solve the continuity eq. (9) and momentum eqs. (2-3).
5. Solve for the temperature distribution from eq. (16). For the control volumes including the interface, the temperature is set to the saturation temperature and eq. (18) is used to determine the mass production rate, $\dot{m}'''$.
6. Compute the source term for the VOF equation (10) and the continuity equation (9).
7. Go back to step 2 until the relative residuals for the pressure correction equation, momentum equations, and enthalpy equation are within the limit.

After the solution for the current time step is obtained, the computation for the next time step is performed. The heat transfer and fluid flow is solved using the SIMPLE Algorithm (Patankar, 1980). The convection-diffusion terms are discretized using a power law scheme. After the grid number test, a non-uniform grid with 44 grid points in x direction and 66 grid points in y direction was used in the numerical solution. After the grid size and the time step test, the problem is solved using a non-uniform grid of $44(x) \times 66(y)$. The grid near the top of the fin is very fine in order to simulate fluid flow and heat transfer in the thin liquid layer. The grid near the right hand side of the fin surface is very fine in order to simulate the effect of contact angle and surface tension on the condensation. After several numerical tests, the false time step used in the computation is $\Delta t = 10^{-7}s$.

RESULTS AND DISCUSSION

Numerical simulations are performed for water at the saturation temperature of 373K. The other geometric parameters are: $L_1 = 0.02mm$, $W = 0.06mm$, $t_g = 0.24mm$, $t_v = 0.54mm$ and $\theta_{mcn} = 84°$. The vapor is assumed to be saturated and therefore there is no heat transfer in the vapor phase. Fig. 2 (a) and (b) show the contour of the VOF of water for temperature drops of $\Delta T = 5K$ and $10K$ respectively. It can be seen that the liquid film thickness on the fin top is very small, and it is therefore expected that heat condensation mainly occurs on the fin top surface. Since the distance between most parts of the liquid vapor meniscus and the cold wall is much larger than the film thickness on the fin top, it is expected tbat, as becomes evident later, the contribution of condensation on the meniscus to the overall heat transfer of the grooved structure is not important. Fig. 3 compares the liquid film thickness obtained by the present numerical solution and the solution of Khrustalev and Faghri (1994b), who assumed that the heat transfer

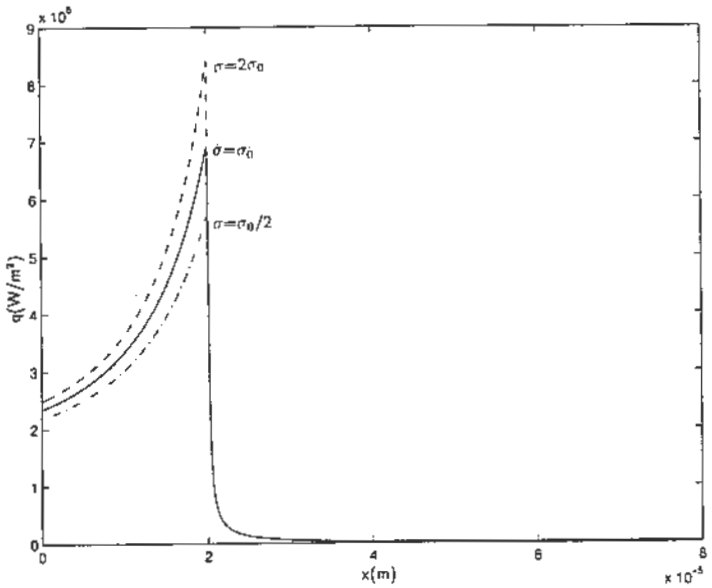

Figure 9. Effect of surface tension on the local heat fluxes

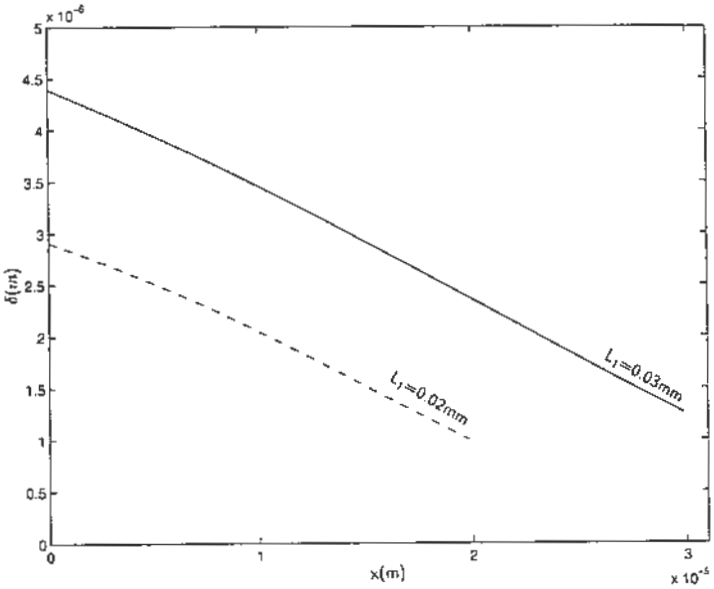

Figure 10. Effect of fin thickness on the liquid film thickness

across the liquid film on the fin top is due to conduction only. It can be seen that the present results agreed very well with that of Khrustalev and Faghri (1994b), which suggests convection has little effect on the film thickness on the fin top.

Fig. 4 (a) and (b) show temperature contours for temperature drops of $\Delta T = 5K$ and $10K$ respectively. It can he seen that the temperature gradient across the thin liquid film on the fin top is very large. On the other hand, the temperature gradient at most parts of the meniscus in the fin is very small. The different behaviors of the temperature gradient on the fin top and the meniscus suggest that condensation occurs mainly on the fin top. Fig. 5 shows the local heat flux on the fin top and the liquid- vapor meniscus for different temperature drops. It can he seen that local heat flux at the fin top surface is higher than that at the meniscus for two order of magnitude. The majority of heat is transferred through condensation on the fin top surface. This is because the thickness of the liquid film on the fin top surface is much thinner than that in the meniscus. When the temperature drop is increased from 5K to 10K, the local heat flux at hoth fin top and meniscus is significantly increased.

Fig. 6 shows the effect of contact angle, θ_{men}, on the liquid film thickness on the fin top. The liquid film thickness at the centerline of the fin decreases with the increasing contact angle. On the other hand, the liquid film thickness at the corner of the fin increases with the increasing contact angle. In other words, increasing the contact angle causes the liquid film on the fin top to become more flat. The effect of the contact angle on the local heat flux is shnwn in Fig. 7. The heat flux is more uniform when the contact angle is increased from 84° to 88°.

The effect of surface tension on the liquid film thickness on the fin top for the temperature drop of 10K is shown in Fig. 8. In addition to the result for surface tension at its normal value, σ_0, two curves with changed surface tension are also plotted in Fig. 8 for comparison. It can he seen that the liquid film thickness on the fin top decreases with increasing surface tension. The reason that film thickness thins with increasing surface tension is that the condensation phenomenon always tends to minimize the surface energy at the interface. With increasing surface tension, this energy increase-. In order to reduce this energy, the radii of curvature has to he increased and that means liquid film thickness has to he decreased. Fig. 9 shows the local heat fluxes for varying surface tension. The maximum heat flux is obtained from the case with the highest surface tension because the liquid film thickness is thinnest for highest surface tension.

The effect of the fin thickness, L_1, on the liquid film thickness of the fin top is shown in Fig. 10. The groove width, W, is decreased by the same value as the increase of the fin thickness to maintain a constant $L_1 + W$ for hoth

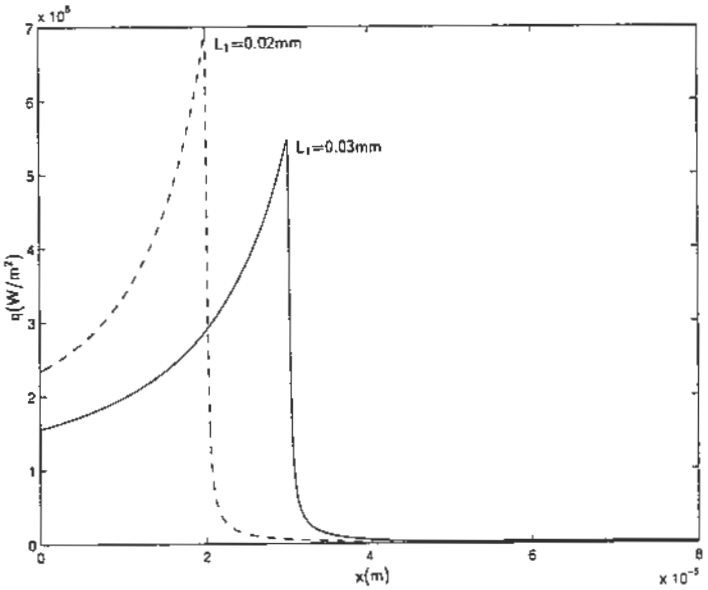

Figure 11. Effect of fin thickness on the local heat fluxes

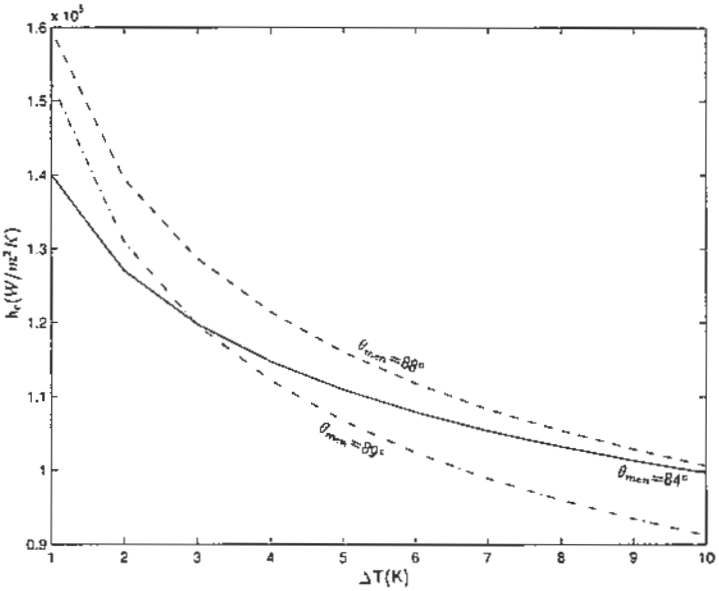

Figure 12. Variation of heat transfer coefficient with temperature drop

cases. In other words, the number of grooves is not changed when the fin thickness, L_1 is increased. As can be seen from Fig. 10, the liquid film thickness increases significantly with increasing fin thickness. Fig. 11 shows the effect of fin thickness on the local heat fluxes. It is seen that the local heat flux is significantly lower for larger fin thickness, because the liquid film is thicker. The effect of fin thickness, however, on the total heat transfer is not as significant as its effect on the local heat flux, because the condensation area is larger for thicker fins.

The heat transfer coefficient defined by eq. (32) is a very important parameter for the design of the grooved structure. The effect of the temperature drop on the heat transfer at different contact angles is shown in Fig. 12. It is seen that the heat transfer coefficient decreases with the increasing temperature drop for all contact angles. When the contact angle is increased from 84° to 88°, the heat transfer coefficient is increased for all temperature drops. This increase is more significant for smaller temperature drops. When the contact angle is increased to 89°, heat transfer at lower temperature drops is increased, but it is decreased for larger temperature drops. In order to investigate the effect of contact angle on the heat transfer coefficient, the variation of heat transfer coefficient with contact angle is plotted in Fig. 13. Increasing the contact angle results in an increase of heat transfer coefficient until it reaches a maximum value. Then heat transfer decreases when the contact angle increases further.

CONCLUSIONS

Condensation in a capillary groove has been investigated using the Volume of Fluid (VOF) model. Condensation on the fin top and meniscus is modeled by using appropriate source terms in continuity, VOF, and energy equations. The results show that convection in liquid has an insignificant effect on the film thickness on the fin top. The majority of the heat is transferred through condensation on the fin top surface, because the thickness of the liquid film on the fin top surface is much thinner than that in the meniscus. The liquid film on the fin top becomes flatter and the heat transfer coefficient on the fin top becomes more uniform when the contact angle is increased. When the surface tension is increased, liquid film on the fin top thins and the local heat flux on the fin top is higher. Increasing the fin thickness causes the thickness of the liquid film to increase significantly. For all contact angels, heat transfer coefficients decrease with increasing temperature drop. There is a contact angle at which the heat transfer coefficient is maximum.

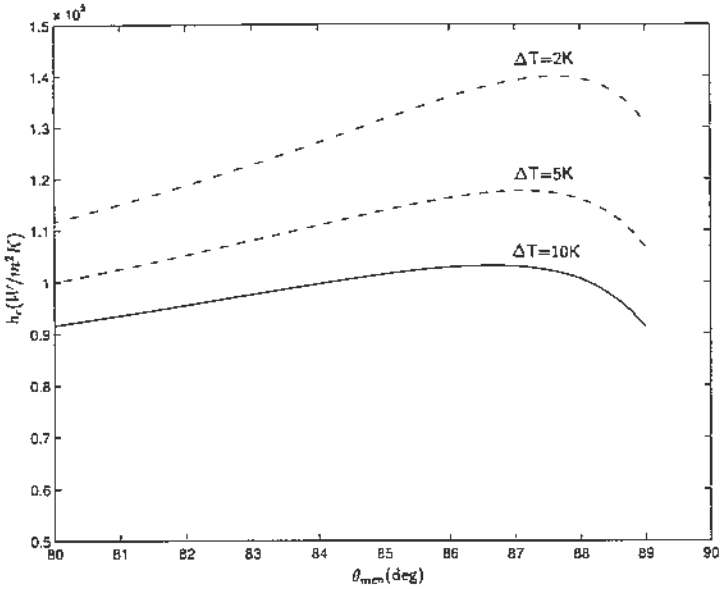

Figure 13. Variation of heat transfer coefficient with contact angle

ACKNOWLEDGMENT

Funding for this work was provided by NASA Grant NAG3-1870 and NSF Grant CTS 9706706.

REFERENCES

Basu, B., and Srinivasan, J., 1988, Numerical Study of Steady State Laser Melting Problem, *Int. J. Heat Mass Transfer*, Vol. 31, pp. 2331-2338.

Brackbill, J.U., Kothe, D.B., and Zemach, C., 1992, A Continuum Method for Modeling Surface Tension, *Journal of Computational Physics*, Vol. 100, pp. 335-354.

Faghri, A., 1995, *Heat Pipe Science and Technology*, Taylor and Francis, Washington, DC.

Kamotani, Y., 1976, Analysis of Axially Grooved Heat Pipe Condensers, AIAA paper No. 76-147.

Khrustalev, D., and Faghri, A., 1994a, Thermal Analysis of a Micro Heat Pipe, *ASME J. Heat Transfer*, Vol. 116, pp. 189-198.

Khrustalev, D., and Faghri, A., 1994b, Heat Transfer During Evaporation and Condensation on Capillary-Grooved Structures of Heat Pipes, Proc. 1994 ASME Winter Annual Meeting, Chicago, Nov., ASME HTD-Vol. 287, pp. 47-59.

Khrustalev, D., and Faghri, A., 1995, Thermal Characteristics of Conventional and Flat Miniature Axially Grooved Heat Pipes, *ASME J. Heat Transfer*, Vol. 117, pp. 1048-1054.

Khrustalev, D., and Faghri, A., 1996, Fluid Flow Effects in Evaporation from Liquid-vapor Meniscus , *ASME J. Heat Transfer*, Vol. 118, pp. 725-730.

Khrustalev, D., and Faghri, A., 1999, Coupled Liquid and Vapor Flow in Miniature Passages with Micro Grooves, *ASME J. Heat Transfer*, Vol. 121, pp. 729-733.

Patankar, S.V., 1980, *Numerical Heat Transfer and Fluid Flow*, McGraw-Hill, New York.